Potential of Favipiravir Analogs as SARS-CoV-2 RdRp Inhibitors: Synthesis and *In Silico* Studies

Anita Alni*, Angela Lokitha, Yusuf Eka Maulana, Elvira Hermawati, and Ade Danova

Organic Chemistry Division, Department of Chemistry, Faculty of Mathematics and Natural Sciences, Institut Teknologi Bandung, Jl. Ganesha No. 10, Bandung 40132, Indonesia

* ***Corresponding author:***

email: alni@itb.ac.id

Received: July 23, 2024
Accepted: October 28, 2025

DOI: 10.22146/ijc.98538

Abstract: *The novel severe acute respiratory syndrome coronavirus-2 (SARS-CoV-2) is responsible for causing the lethal infectious disease known as COVID-19. The RNA-dependent RNA polymerase (RdRp) is a pivotal component that facilitates the translation of viral RNA into viral proteins. Therefore, our study aimed to synthesize new inhibitors from favipiravir (FVP) analogs by modifying the hydrophobicity through a nucleophilic aromatic substitution at the C-6 position of the pyrazine ring with alkoxy groups under acidic conditions. Moreover, the synthesized FVP analogs were investigated for their antiviral potency against SARS-CoV-2 RdRp through* in silico *studies. Five FVP analogs (**3**–**7**), including four known (**3**, **4**, **5**, **7**) and one new (**6**), were successfully synthesized with yields ranging from 2.3 to 32.7%. All favipiravir analogs could be drug-likeness with inactive hepatotoxicity and carcinogenicity. The docking study showed that compound **5** exhibited a strong binding affinity with a binding score of −7.00 kcal/mol by interacting with the catalytic site residues of Asp618 and Asp760 of SARS-CoV-2 RdRp. Furthermore, the molecular dynamics simulation revealed that the compound **5** was stable, as indicated by RMSD, Rg, solute H-bonds, RMSF, and binding energy calculations. Thus, these results suggest that the FVP-RTP analog (**5**) may have antiviral potency by targeting SARS-CoV-2 RdRp.*

Keywords: *favipiravir; COVID-19; SARS-CoV-2 RdRp; molecular docking; molecular dynamics simulation*

■ INTRODUCTION

Coronavirus disease 2019, commonly known as COVID-19, is a severe infectious disease caused by the novel severe acute respiratory syndrome coronavirus 2 (SARS-CoV-2). First identified in Hubei Province, Central Eastern China, in December 2019, the disease has since spread globally, leading to widespread panic and accelerating efforts to combat it [1-2]. Although vaccination rates have been high, vulnerable individuals are still at risk of severe health consequences. Antiviral and immunomodulatory drugs are crucial for treating vulnerable patients. SARS-CoV-2 belongs to the family *Coronaviridae*, specifically to the genus Beta-coronavirus, and has a positive-sense RNA genome that ranges in length from 29.8 to 29.9 kB [3-4]. SARS-CoV-2 depends on its RNA-dependent RNA polymerase (RdRp) to replicate its genetic material. This enzyme is also critical for transcribing viral RNA into viral proteins [5-6]. Moreover, remdesivir and favipiravir are two nucleoside analogs that have been shown to inhibit viral replication by incorporating into the growing viral RNA chain and causing chain termination [7-8].

In a previous study, favipiravir (FVP) was reported to have broad antiviral activity at higher concentrations against many other RNA viruses [9-11]. Recent studies have shown that SARS-CoV-2 has acquired phenotypic resistance to Remdesivir and PaxlovidTM [12], except for favipiravir. In addition, favipiravir is known as a pro-drug that must be first converted by hypoxanthine-guanine phosphoribosyltransferase (HGPRT) to FVP-ribosyl-5'-monophosphate (FVP-RMP) and then metabolized to the FVP-ribofuranosyl-5'-triphosphate

(FVP-RTP) by cellular kinases [12-13] to inhibit the enzyme. Although this inhibitor has relatively low antiviral activity, a large oral dose is necessary for clinical use [14]. Moreover, FVP is easily modifiable while maintaining its unique mode of action because of its relatively simple structure. Thus, additional structural modifications of favipiravir and pyrazine are necessary [15-16]. Based on the *in silico* studies, Latosińska and Latosińska reported that two FVP analogs possessing -CF_3 and -CN at the C-6 position of the pyrazine ring exhibited a strong binding affinity for the RNA template, RNA primer, cofactors, and RdRp, which suggested that they could serve as effective alternatives to favipiravir [15]. In our recent study, we aimed to modify lipophilicity by altering the substituents at the C-6 position of the pyrazine ring with alkoxy using a nucleophilic aromatic substitution (S_NAr) and evaluate the FVP analogs for their potential use. *In silico* studies were conducted to assess the potential of FVP analogs as antiviral agents against COVID-19, with a focus on their binding efficiency and stability within the SARS-CoV-2 RdRp in aqueous conditions.

■ EXPERIMENTAL SECTION

Materials

All chemicals were acquired from commercial suppliers and used without further purification. All the solvents were sourced from non-commercial sources and were subsequently purified for further use. Silica gel for column chromatography (0.063–0.200 mm) was purchased from Merck Company. Thin-layer chromatography (TLC) was conducted on Merck TLC plates (0.23 mm thickness) and visualized by UV light.

Instrumentation

NMR measurements were performed using Agilent Varian DD2 500 MHz spectrometers (Agilent, USA). Mass spectra (MS) were taken on high-resolution mass spectrometry (HRMS) Waters LCT Premier XE ESI-TOF-MS (Waters, USA).

Procedure

Synthesis of favipiravir analogs (3–7)

The favipiravir analogs were synthesized using a previous method [16]. First, 6-fluoro-3-hydroxy-pyrazine-2-carboxamide (0.30 g, 1.9 mmol) and alcohol (5 mL) were mixed in the carousel tube at room temperature. Then, 0.96 mL of HCl in dioxan (4.0 M) was added dropwise. The reaction was stirred at room temperature for 1–24 h or refluxed for 1–3 h, and then continued by stirring for an additional 1 h. The reaction was monitored by TLC. After that, water was added dropwise until a precipitate formed, or the extract was purified using ethyl acetate and then further purified using radial/column chromatography. The pure products were characterized using ^{1}H-NMR, ^{13}C-NMR, and HRMS. All NMR and MS spectra are available in the supplementary material.

In silico *studies*

ADME, drug-likeness, and toxicology prediction. The SwissADME web-based tool was employed to predict the physicochemical and ADME properties of compounds **1**–**7** [17]. Toxicology assessment was predicted using the ProTox 3.0 web server (https://tox.charite.de/protox3/) [18]. The SMILES for these compounds were generated using ChemOffice Professional 15.0 and subsequently submitted to SwissADME for analysis.

Molecular docking. Molecular docking was conducted using PyRx (version 1.1) virtual screening software based on the AutoDock V.4.2.6 [19-20]. The complex structures of SARS-CoV-2 with ligand were retrieved from the RSCB Protein Databank with PDB ID 7CTT. Before docking the candidate ligands, the native ligand that crystallized with the RNA was removed from the structure, and water was removed using Discovery Studio software. The redocking process of the native ligand was conducted to validate the docking method using AutoDock by docking into the active site of the SARS-CoV-2 receptor to obtain the RMSD value ≤ 2.0 Å [21]. The grid box center was set to coordinates (x, y, z) = (123.680, 124.324, 129.415) with a grid spacing of (x, y, z) = (20, 20, 20) Å. The AutoDock calculations were carried out in two separate steps: 1) the pre-calculation of atomic affinities with AutoGrid, and 2) ligands were docked utilizing AutoDock with Lamarckian Genetic Algorithm (LGA). The use of Automatic Docking with AutoGrid was used to pre-calculate the grids for each

atom type in the ligand. The pre-calculated grids were used as a template. The tested ligands were docked into the active site of the SARS-CoV-2 receptor, using a box size and location identical to those of the native ligand.

Molecular dynamics simulation. Molecular dynamics simulations were performed on the selected molecules using the YASARA Structure package (version 21.6.17) with the AMBER14 force field [22-24]. The simulations revealed the structural integrity and conformational changes in the protein-ligand docked complex. Prior to the simulation, a series of preparations, including hydrogenation, optimization, and calibration, were performed. The initial energy of the system was minimized before the operating temperature was maintained at 298 K and 0.997 g/mL (water density) for the duration of the MD simulation. The complex was placed in a water box with dimensions of 100.0 × 100.0 × 100.0 Å along the x-, y-, and z-axes, and periodic boundary conditions were applied. The Particle-Mesh Ewald algorithm, with a cutoff of 8.0 Å, was used to calculate the Coulomb forces. The simulation was conducted using a time step of 2 × 1.25 fs (normal speed). Trajectory data were saved at 100-ps intervals throughout the 100-ns simulation.

■ RESULTS AND DISCUSSION

Synthesis of Favipiravir Analogs

Five synthesized FVP analogs (**3**–**7**), including four known (**3**, **4**, **5**, **7**) and one new (**6**), were successfully prepared using a previously reported method [16] that utilized favipiravir as the starting material, as shown in Scheme 1. FVP in this research was obtained from our work, which had been reported in a patent with the number 2024/01553 in Indonesia, using Selectfluor® as a fluorinating agent [25-27]. FVP was reacted with aliphatic alcohol, catalyzed by 4.0 M HCl in dioxane, yielding a range of 2.3–32.7% as presented in Table 1. Among five FVP analogs (**3**–**7**), three compounds (**3**, **6**, **7**) were easily precipitated by adding water to yield 21.7, 32.7, and 3.9%, respectively. Nevertheless, the compound **4** was obtained using radial chromatography with an eluent gradient of 100% *n*-hexane to 60% *n*-hexane in ethyl acetate, yielding 2.3% of the compound. Additionally, compound **5** was purified using column chromatography with an eluent gradient of 100% chloroform to 80% chloroform in methanol, yielding 7.5% of the compound. All synthesized compounds of this study were obtained with modest yield. This result could be caused by the formation of a highly protonated favipiravir salt, which would decrease its reactivity. Moreover, the use of a dry solvent and inert conditions is required in this reaction [16].

To address the structure elucidation of the new compound (**6**) as presented in Fig. 1, ^{1}H- and ^{13}C NMR spectroscopy, as well as MS, were conducted. The ^{1}H-NMR spectra showed a proton doublet at 1.03 ppm, which belonged to two methyl groups close to the methine group, with a coupling constant of 6.7 Hz. The proton signals of methine and methylene groups appeared as multiplets and doublets at 2.11 and 4.01 ppm, respectively. The proton of hydroxy attached to the pyrazine ring showed a singlet at 11.9 ppm. However, the proton of the NH_2 group appeared as two singlet signals at 5.92 and 7.43 ppm, where one proton was downfield due to a hydrogen bonding interaction

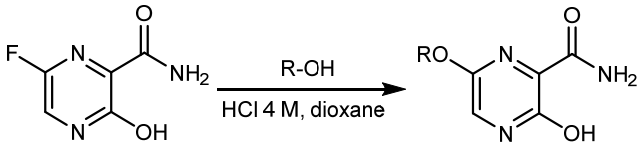

Scheme 1. Synthesis of favipiravir analogs (**3**–**7**)

Table 1. The result of the synthesis of favipiravir analogs (**3**–**7**)

Compounds	OR	Condition (temp, time)	%Yield
3	$-OCH_3$	rt, 21 h	21.7%
4	$-OCH_2CH_3$	rt, 21 h	2.3%
5	$-OCH(CH_3)_2$	60 °C, 4 h	7.5%
6	$-OCH_2CH(CH_3)_2$	60 °C, 6 h	32.7%
7	$-OCH_2CH_2OCH_3$	rt, 21 h	3.9%

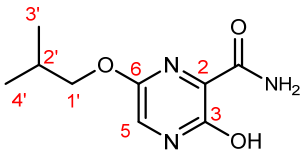

Fig 1. Structure of compound **6**

with the hydroxy group [28]. Moreover, the proton signal of the CH-sp^2 group belonging to the pyrazine ring showed a singlet at 8.13 ppm, which confirmed that the fluorine atom had been replaced with an alkoxy group to form favipiravir analogs. In addition, the HMBC experiment showed a correlation between the proton of the CH_2 group at 4.01 ppm and the oxygenated carbon of the C-6 position at 153.6 ppm, as presented in Table 2, indicating that the alkoxy group was attached to the carbon at the C-6 position. Besides, the result of high-resolution mass spectrometry for compound **6** was found to be 212.1027 *m/z* for $C_9H_{14}N_3O_3^+$ (calc. for $C_9H_{14}N_3O_3^+$: 212.1030 *m/z*). Furthermore, the results of ^{1}H- and ^{13}C-NMR spectroscopy for compounds **3**–**5** and **7** are summarized in Tables 3 and 4. Additionally, all the known compounds (**3**–**5**, **7**) have been reported by Song et al. [16].

In Silico Studies

ADME predictions

In silico ADME refers to the use of computational methods and models to predict the pharmacokinetic properties of drug candidates during the early stages of drug discovery. Understanding the ADME characteristics of a compound is crucial for identifying potential drug candidates with favorable bioavailability, distribution, metabolism, and elimination properties. *In silico* ADME predictions serve as complementary tools to experimental assays, aiding in the prioritization of compounds for further development [29-31]. In this study, ADME predictions were evaluated based on five criteria for drug-likeness, including molecular weight (MW), log P, solubility, bioavailability, topological polar surface area (TPSA), and gastrointestinal absorption (GI). Moreover, toxicology profiles were predicted, namely hepatotoxicity and carcinogenicity.

Table 2. The result of ^{1}H-, ^{13}C-NMR, and HMBC correlation of compound **6**

No. C	δ_C*	δ_H (*m*, *J* (Hz))*	HMBC (H→C)
2	139.7	-	-
3	157.5	-	-
5	119.4	8.13 (*s*, 1H)	C-3
6	153.6	-	-
1'	73.1	4.01 (*d*, 2H, *J* = 6.6)	C-6, C-3', C-4'
2'	27.8	2.11 (*m*, 1H)	C-1', C-3', C-4'
3'	19.1	1.03 (*d*, 6H, *J* = 6.7)	C-1', C-2', C-4
4'	19.1	1.03 (*d*, 6H, *J* = 6.7)	C-1', C-2', C-3'
$-CONH_2$	170.0	5.92 (*s*, 1H) 7.43 (*s*, 1H)	-
–OH	-	11.90 (*s*, 1H)	-

* ^{1}H- and ^{13}C-NMR spectroscopy at 500 and 125 MHz in $CDCl_3$

Table 3. The summary of ^{1}H- and ^{13}C-NMR of compounds **3** and **4**

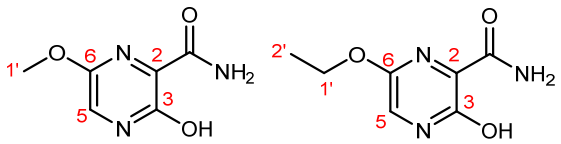

3 **4**

Compound **3***			Compound **4***		
No. C	δ_C	δ_H (*m*, *J* (Hz))	No. C	δ_C	δ_H (*m*, *J* (Hz))
2	138.4	-	2	138.5	-
3	157.7	-	3	157.5	-
5	120.9	8.16 (*s*, 1H)	5	120.9	8.13 (*s*, 1H)
6	153.8	-	6	153.5	-
1'	54.6	3.93 (*s*, 3H)	1'	62.9	4.38 (*q*, 2H, *J* = 7.05)
$-CONH_2$	170.4	8.37 (*s*, 1H) 8.54 (*s*, 1H)	2'	14.8	1.31 (*t*, 3H, *J* = 7.05)
–OH	-	12.78 (*s*, 1H)	$-CONH_2$	170.5	8.35 (*s*, 1H) 8.52 (*s*, 1H)
			–OH	-	12.78 (*s*, 1H)

* ^{1}H- and ^{13}C-NMR spectroscopy at 500 and 125 MHz in $CDCl_3$

Table 4. The summary of ^{1}H- and ^{13}C-NMR of compounds **5** and **7**

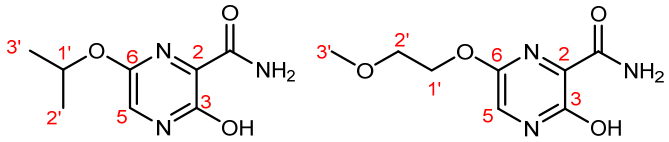

5 **7**

Compound **5**[*]			Compound **7**[*]		
No. C	δ_C	δ_H (*m*, *J* (Hz))	No. C	δ_C	δ_H (*m*, *J* (Hz))
2	138.7	-	2	143.3	-
3	157.6	-	3	162.4	-
5	121.1	8.05 (*s*, 1H)	5	125.6	8.17 (*s*, 1H)
6	152.7	-	6	158.1	-
1'	22.2	5.36 (*m*, 1H)	1'	70.9	3.65 (*t*, 2H, *J* = 4.45)
2'	70.2	1.27 (*d*, 6H, *J* = 6.10)	2'	75.3	4.48 (*t*, 2H, *J* = 4.45)
3'	69.3	1.27 (*d*, 6H, *J* = 6.10)	3'	63.3	3.32 (*s*, 3H)
$-CONH_2$	170.4	8.29 (*s*, 1H) 8.58 (*s*, 1H)	$-CONH_2$	175.2	8.36 (*s*, 1H) 8.58 (*s*, 1H)
−OH	-	12.78 (*s*, 1H)	−OH	-	12.79 (*s*, 1H)

[*] ^{1}H- and ^{13}C-NMR spectroscopy at 500 and 125 MHz in $CDCl_3$

Table 5. The physicochemical properties of the favipiravir analogs

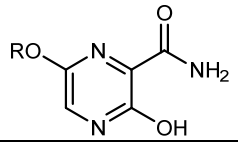

OR	MW	Log P	Solubility	Bioavailability	TPSA (A^2)	GI	Drug-likeness	Hepatotoxicity	Carcinogenicity
F (FVP)	157.10	−0.16	Soluble	0.55	89.10	High	Yes	Inactive	Inactive
H	139.11	−0.60	Soluble	0.55	89.10	High	Yes	Inactive	Inactive
$-OCH_3$	169.14	−0.37	Soluble	0.55	98.33	High	Yes	Inactive	Inactive
$-OCH_2CH_3$	189.16	−0.04	Soluble	0.55	98.33	High	Yes	Inactive	Inactive
$-OCH(CH_3)_2$	197.19	0.23	Soluble	0.55	98.33	High	Yes	Inactive	Inactive
$-OCH_2CH(CH_3)_2$	211.22	0.59	Soluble	0.55	98.33	High	Yes	Inactive	Inactive
$-OCH_2CH_2OCH_3$	213.19	−0.35	Soluble	0.55	107.56	High	Yes	Inactive	Inactive

As presented in Table 5, the MW of the FVP analogs (**3**–**7**) was all below 500 g/mol. SwissADME prediction indicated that the FVP analogs (**3**–**7**) showed a log P value ranging from −0.37 to 0.59, suggesting high water solubility for all FVP analogs. The methoxy and ethoxy analogs, such as FVP, showed low and negative lipophilicity. Meanwhile, the isopropoxy (**5**), isobutoxy (**6**), and 2-ethoxyethoxy (**7**) analogs exhibited positive lipophilicity, with isobutoxy (**6**) showing the highest and most positive lipophilicity. The substitution of F with isopropoxy enhanced the lipophilicity of the FVP analogs, demonstrating the potential for altering lipophilicity to target hydrophobic sites.

Furthermore, the FVP analogs demonstrated high GI and bioavailability values with a probability of 55%. The TPSA, which characterizes passive molecular transport across cell membranes, was 98.33, except for compound **7**, which displayed a significantly higher TPSA of 107.56; however, it did not exceed 140. As a result, there were no violations of the drug-likeness rules indicative of lead-likeness. In addition, toxicology prediction indicated that favipiravir (**1**) and its analogs

(**2**–**7**) were classified as inactive hepatotoxicity and carcinogenicity.

Molecular docking

Molecular docking was conducted for the triphosphorylated forms of the favipiravir analogs (FVP-RTP) by targeting SARS-CoV-2 RdRp (RNA-dependent RNA polymerase). All FVP-RTP analogs were docked together into the active site of SARS-CoV-2 RdRp using PyRx virtual screening (AutoDock v4.2.6). In this study, a more negative binding score indicates high binding affinity, while a more positive binding score indicates low binding affinity. According to Table 6, FVP-RTP (**1**) showed the highest binding affinity and inhibition constants (K_i) with values of −8.88 kcal/mol and 0.31 μM, respectively. Among all FVP-RTP analogs, compound **5** exhibited the highest binding affinity and K_i values of −7.00 kcal/mol and 7.34 μM, respectively, compared with the others. This indicated that binding affinity was associated with the inhibition constant. Compounds **3** and **4**, which possess methoxy and ethoxy groups, showed a lower binding affinity compared with compound **2**. Moreover, the introduction of isobutoxy (**6**) and 2-methoxyethoxy (**7**) groups enhanced the binding score, with values of −5.83 and −5.65 kcal/mol, respectively, compared with compound **5**. This result suggested that compound **5**, possessing isopropyl, could be the best hydrophobic property to enhance binding affinity in the active site of SARS-CoV-2 RdRp. Moreover, compounds with a minimum binding energy of ≤ −6 kcal/mol were classified as active or hit molecules, in line with previous reports [32-33].

To address the binding interaction of FVP-RTP (**1**) and FVP-RTP analog (**5**), a 2D interaction of ligand-protein was prepared using BIOVIA Discovery Studio Visualizer. The redocking procedure produced a root-mean-square deviation (RMSD) of 1.75 Å compared to the native ligand's position in the co-crystallized FVP-RTP structure (Fig. 2). As shown in Fig. 3(a), the complex of FVP-RTP (**1**) with SARS-CoV-2 RdRp exhibited eight hydrogen bonding interactions with four amino acid residues (Cys622, Asp623, Ser682, and Asn691) and RNA (C10T). The ionic interaction showed significantly with residues Arg553, Arg555, Lys621, and Lys798. Moreover, the Van der Waals interaction had three interactions with RNA (U11T and A20Q), as well as Asp760. This result demonstrated that hydrogen bonding and ionic interactions could be the key interactions for stabilizing the complex of FPV-RTP with SARS-CoV-2 RdRp in the active site [15].

Furthermore, 2D interaction of the complex of FPV-RTP analog (**5**) with SARS-CoV-2 RdRp (Fig. 3(b)) displayed twelve hydrogen bonding interactions with six amino acid residues (Lys545, Arg553, Arg555, Lys621, Cys622, Lys798) and RNA (A20Q). Additionally, π-ionic

Table 6. The binding energy and inhibition constant of FVP-RTP analogs

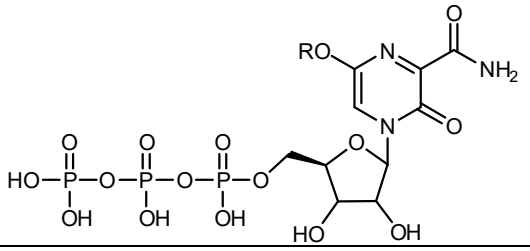

OR	Binding score (kcal/mol)	K_i (μM)
F (FVP)*	−8.88	0.31
H	−6.37	21.42
$-CH_3$	−5.82	54.42
$-CH_2CH_3$	−5.57	82.83
$-CH(CH_3)_2$	−7.00	7.34
$-CH_2CH(CH_3)_2$	−5.83	53.03
$-CH_2CH_2OCH_3$	−5.02	210.27

*Redocking

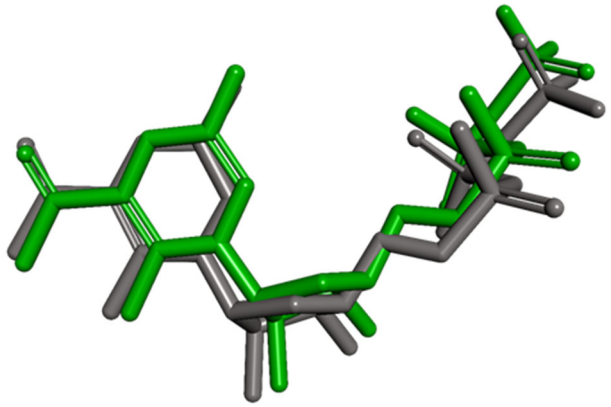

Fig 2. Superimpose co-crystallized FVP-RTP (grey) and redocking FVP-RTP (green)

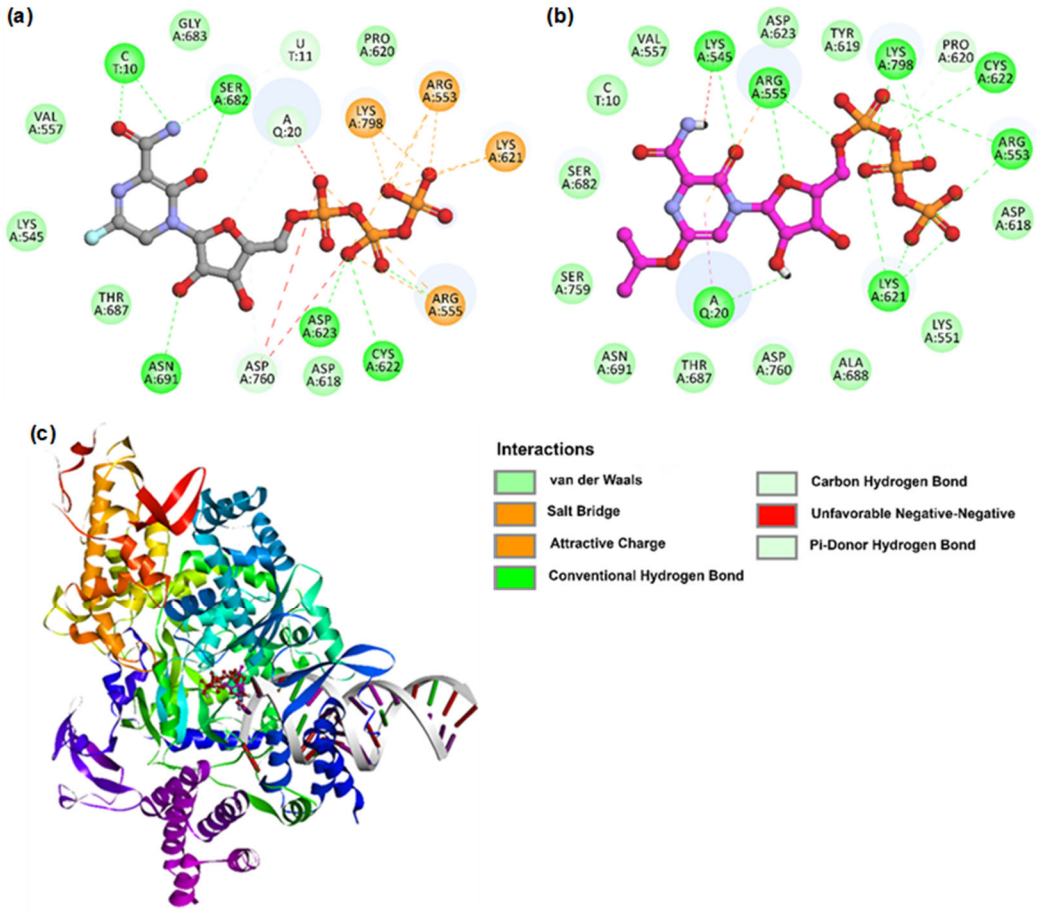

Fig 3. Two-dimensional ligand–protein interaction profiles and superimposition of (a) favipiravir (**1**) and (b) its analogs (**5**) in (c) complex with SARS-CoV-2 RdRp (7CCT)

and π-π interactions were observed with Arg555 and RNA (A20Q). Notably, this compound also interacts with the catalytic site residues Asp618 and Asp760 [34]. This finding suggests that the presence of a hydrogen bonding interaction in the complex of FVP-RTP analogs with SARS-CoV-2 RdRp may be a crucial interaction for stabilizing the complex form (Fig. 3(c)) [33,35-36].

Molecular dynamics simulation

Molecular dynamics simulation is a computationally appealing approach for evaluating the stability of protein-ligand complexes over time, considering a range of parameters [37]. In this study, four parameters were used to investigate the stability of protein-ligand complexes, such as RMSD, radius of gyration (Rg), binding energy, the number of solute H-bonds, and root-mean-square-fluctuation (RMSF). As shown in Fig. 4(a), the RMSD values of both complexes of the FVP-RTP analog (**5**) with 7CCT and FVP with SARS-CoV-2 RdRp showed slight fluctuations, and the average for both complexes was approximately 2.24 and 1.94 Å, respectively. Furthermore, the measurements of the Rg and the number of hydrogen bonds for both complexes showed no significant difference, as depicted in Fig. 4(c) and 4(d). Therefore, these results indicate that both complexes were stable [33,36]. As shown in Fig. 4(b), the binding energy of the FVP-RTP complex with SARS-CoV-2 RdRp remained consistent around −1349.29 kJ/mol. Moreover, the average binding energy of the FVP-RTP analog (**5**) complex with SARS-CoV-2 RdRp (−1744.75 kcal/mol) was lower compared with FVP-RTP. However, the ligand-protein interactions were not as stable as those of FVP-RTP. The RMSF analysis provides insights into the flexibility of amino acid residues during the molecular dynamics simulation. As shown in Fig. 4(e),

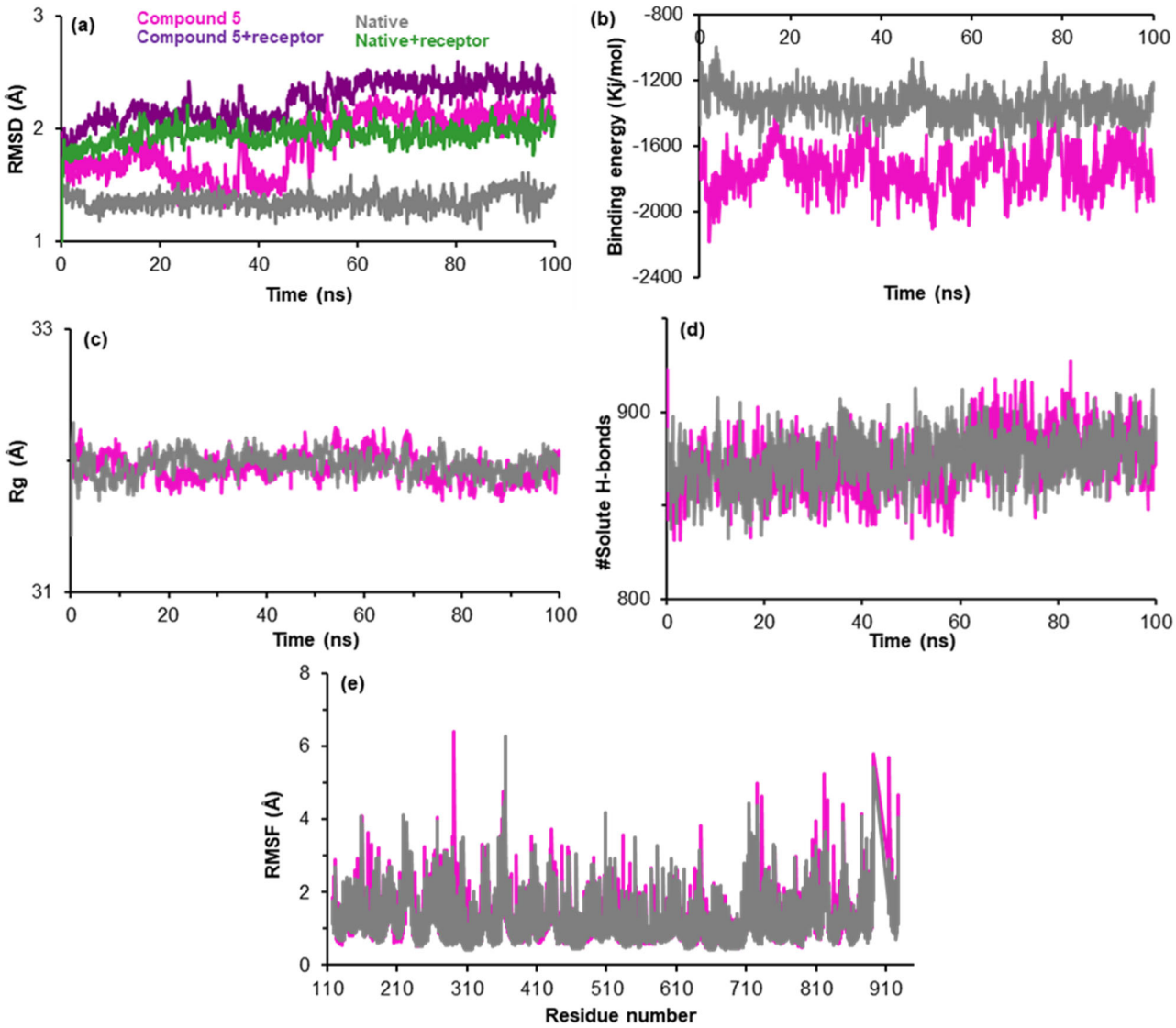

Fig 4. Time evolution of (a) RMSD, (b) binding energy, (c) Rg, (d) #solute H-bonds, and (e) RMSF of FVP-RTP analog (**5**) in complex with the SARS-CoV-2 RdRp (7CCT)

FVP-RTP analog (**5**) and FVP-RTP exhibited generally similar fluctuation patterns across the entire protein, particularly in the binding site residues (545–798). These results suggested that the FVP-RTP analog (**5**) could be a potential inhibitor of SARS-CoV-2 RdRp and warrant further investigation through *in vitro* and *in vivo* studies to confirm its efficacy.

■ CONCLUSION

To summarize, five FVP analogs (**3-7**), including four known (**3**, **4**, **5**, **7**) and one new (**6**), were synthesized via nucleophilic aromatic substitution in acidic conditions, yielding 2.3–32.7% of the target compounds. Moreover, seven compounds (**1**–**7**) including favipiravir (**1**), 3-hydroxy-pyrazine-2-carboxamide (**2**), and favipiravir analogs (**3**–**7**) were investigated their inhibitory potency against SARS-CoV-2 RdRp using *in silico* studies, such as drug-likeness MW, log P, solubility, bioavailability, TPSA, and GI, toxicology assessment (hepatotoxicity and carcinogenicity), molecular docking, and molecular dynamics simulation. All compounds obey Lipinski's rule, exhibit inactive hepatotoxicity, and are inactive in terms of carcinogenicity. Molecular docking indicated that compound **5** showed a high binding affinity, with a

binding score and K_i value of −7.0 kcal/mol and 7.34 μM, respectively. Compound **5** exhibited twelve H-bond interactions with six amino acid residues and one RNA, specifically Lys545, Arg553, Arg555, Lys621, Cys622, and Lys798, as well as RNA (A20Q). Molecular dynamics simulation suggested that compound **5** was stable in complex with SARS-CoV-2 RdRp based on root-mean-square deviation, binding energy, radius of gyration, number of solute H-bonds, and RMSF during simulation. Thus, compound **5** may be a potent antiviral drug against SARS-CoV-2 RdRp. Further *in vitro* and *in vivo* assays are required to validate this hypothesis.

■ ACKNOWLEDGMENTS

We are grateful for financial support from the National Research and Innovation Agency (BRIN) and Indonesia Endowment Fund for Education (LPDP) through the research grant *"Riset dan Inovasi untuk Indonesia Maju (RIIM)"*, contract number 20/IVKS/06/2022 and 417/IT1.B07/KS.00/2022.

■ CONFLICT OF INTEREST

The authors have no conflict of interest.

■ AUTHOR CONTRIBUTIONS

Angela Lokitha and Yusuf Eka Maulana synthesized and evaluated by an *in silico* study. Ade Danova, Anita Alni, and Elvira Hermawati conceived, supervised, and designed the study. Ade Danova and Anita Alni wrote and revised the main manuscript. All the authors have read and agreed to the final version of the manuscript.

■ REFERENCES

[1] Perlman, S., 2020, Another decade, another coronavirus, *N. Engl. J. Med.*, 382 (2), 760–762.

[2] Zhang, T., Wu, Q., and Zhang, Z., 2020, Probable pangolin origin of SARS-CoV-2 associated with the COVID-19 outbreak, *Curr. Biol.*, 30 (7), 1346–1351.e2.

[3] Khailany, R.A., Safdar, M., and Ozaslan, M., 2020, Genomic characterization of a novel SARS-CoV-2, *Gene Rep.*, 19, 100682.

[4] Wang, C., Liu, Z., Chen, Z., Huang, X., Xu, M., He, T., and Zhang, Z., 2020, The establishment of reference sequence for SARS-CoV-2 and variation analysis, *J. Med. Virol.*, 92 (6), 667–674.

[5] Hillen, H.S., Kokic, G., Farnung, L., Dienemann, C., Tegunov, D., and Cramer, P., 2020, Structure of replicating SARS-CoV-2 polymerase, *Nature*, 584 (7819), 154–156.

[6] Arba, M., Nur-Hidayat, A., Usman, I., Yanuar, A., Wahyudi, S.T., Fleischer, G., Brunt, D.J., and Wu, C., 2020, Virtual screening of the Indonesian medicinal plant and zinc databases for potential inhibitors of the RNA-dependent RNA polymerase (RdRp) of 2019 novel coronavirus, *Indones. J. Chem.*, 20 (6), 1430–1440.

[7] Kokic, G., Hillen, H.S., Tegunov, D., Dienemann, C., Seitz, F., Schmitzova, J., Farnung, L., Siewert, A., Höbartner, C. and Cramer, P., 2021, Mechanism of SARS-CoV-2 polymerase stalling by remdesivir, *Nat. Commun.*, 12 (1), 279.

[8] McMahon, J.H., Lau, J.S.Y., Coldham, A., Roney, J., Hagenauer, M., Price, S., Bryant, M., Garlick, J., Paterson, A., Lee, S.J., O'Bryan, J., Hearps, A., Tachedjian, G., Pinskier, H., Phillips, C., Garrow, S., Pinskier, N., Melvin, R., Blakeway, L., Wisniewski, J.A., Byers, S., Badoordeen, G.Z., Pereira, S., Pragastis, K., Trubiano, J.A., Chua, K.Y.L., Kainer, M., Molton, J.S., Gardiner, B.J., Pierce, A.B., Cheng, A., Rogers, B.A., and Peleg, A.Y., 2022, Favipiravir in early symptomatic COVID-19, a randomised placebo-controlled trial, *EClinicalMedicine*, 54, 101703.

[9] Watanabe, M., 2020, The COVID-19 pandemic in Japan, *Surg. Today*, 50 (8), 787–793.

[10] Kumar, R., Gupta, N., Kodan, P., Mittal, A., Soneja, M., and Wig, N., 2020, Battling COVID-19: Using old weapons for a new enemy, *Trop. Dis., Travel Med. Vaccines*, 6 (1), 6.

[11] Yavuz, S., and Ünal, S., 2020, Antiviral treatment of COVID-19, *Turk. J. Med. Sci.*, 50, 611–619.

[12] Celik, I., Erol, M., and Tallei, T.E., 2024, "Chapter 39 - *In silico* studies of established antivirals targeting the SARS-CoV-2 RNA-dependent RNA polymerase" in Features, Transmission, Detection, and Case Studies in COVID-19, Eds. Rajendram, R.,

Preedy, V.R., and Patel, V.B., Academic Press, Cambridge, MA, US, 475–487.

[13] Hayden, F.G., Lenk, R.P., Stonis, L., Oldham-Creamer, C., Kang, L.L., and Epstein, C., 2022, Favipiravir treatment of uncomplicated influenza in adults: results of two phase 3, randomized, double-blind, placebo-controlled trials, *J. Infect. Dis*., 226 (10), 1790–1799.

[14] Kaptein, S.J., Jacobs, S., Langendries, L., Seldeslachts, L., ter Horst, S., Liesenborghs, L., Hens, B., Vergote, V., Heylen, E., Barthelemy, K., Maas, E., De Keyzer, C., Bervoets, L., Rymenants, J., Van Buyten, T., Zhang, X., Abdelnabi, R., Pang, J., Williams, R., Thibaut, H.J., Dallmeier, K., Boudewijns, R., Wouters, J., Augustijns, P., Verougstraete, N., Cawthorne, C., Breuer, J., Solas, C., Weynand, B., Annaert, P., Spriet, I., Vande Velde, G., Neyts, J., Rocha-Pereira, J., and Delang, L., 2020, Favipiravir at high doses has potent antiviral activity in SARS-CoV-2–infected hamsters, whereas hydroxychloroquine lacks activity, *Proc. Natl. Acad. Sci. U. S. A.*, 117 (43), 26955–26965.

[15] Latosińska, M., and Latosińska, J.N., 2024, Favipiravir analogues as inhibitors of SARS-CoV-2 RNA-dependent RNA polymerase, combined quantum chemical modeling, quantitative structure–property relationship, and molecular docking study, *Molecules,* 29 (2), 441.

[16] Song, Y., Xu, L., Wang, B., Zhang, D., and Wang, H., 2021, Convenient one-step synthesis of alkoxy substituted pyrazine derivatives, *Results Chem*., 3, 100191.

[17] Daina, A., Michielin, O., and Zoete, V., 2017, SwissADME: A free web tool to evaluate pharmacokinetics, drug-likeness and medicinal chemistry friendliness of small molecules, *Sci. Rep*., 7 (1), 42717.

[18] Banerjee, P., Kemmler, E., Dunkel, M., and Preissner, R., 2024, ProTox 3.0: A webserver for the prediction of toxicity of chemicals, *Nucleic Acids Res*., 52, W513–W520.

[19] Trott, O., and Olson, A.J., 2010, AutoDock Vina: Improving the speed and accuracy of docking with a new scoring function, efficient optimization, and multithreading, *J. Comput. Chem*., 31 (2), 455–461.

[20] Dallakyan, S., and Olson, A.J., 2015, "Small-Molecule Library Screening by Docking with PyRx" in *Chemical Biology: Methods and Protocols*, Eds. Hempel, J.E., Williams, C.H., and Hong, C.C., Humana Press, New York, NY, US, 243–250.

[21] Khatimah, H., Hermawati, E., Mulya, F., Abdjan, M.I., Kuamit, T., and Danova, A., 2025, A new ursane-type pentacyclic triterpenoid from the tree bark of *Sandoricum koetjape*: Antibacterial, DFT, and molecular docking study, *Int. J. Mol. Sci*., 26 (21), 10389.

[22] Duan, Y., Wu, C., Chowdhury, S., Lee, M.C., Xiong, G., Zhang, W., Yang, R., Cieplak, P., Luo, R., Lee, T., Caldwell, J., Wang, J., and Kollman, P., 2003, A point-charge force field for molecular mechanics simulations of proteins based on condensed-phase quantum mechanical calculations, *J. Comput. Chem*., 24 (16), 1999–2012.

[23] Krieger, E., Darden, T., Nabuurs, S.B., Finkelstein, A., and Vriend, G., 2004, Making optimal use of empirical energy functions: Force-field parameterization in crystal space, *Proteins: Struct., Funct., Bioinf.*, 57 (4), 678–683.

[24] Krieger, E., and Vriend, G., 2015, New ways to boost molecular dynamics simulations, *J. Comput. Chem*., 36 (13), 996–1007.

[25] Banik, S., Adarsh, D.R., and Reddy, B.V.S., 2023, Three-step process for the synthesis of favipiravir, *Results Chem.*, 5, 100895.

[26] Fuentes, G., García, M.F., Cerecetto, H., Álvarez, G., Couto, M., and Romero, A.H., 2023, One-step synthesis of favipiravir from Selectfluor® and 3-hydroxy-2-pyrazinecarboxamide in an ionic liquid, *Org. Biomol. Chem*., 21 (17), 3660–3668.

[27] Rachmadhaningtiyas, D.A., Hermawati, E., Juliawaty, L.D., and Wahyuningrum, D., 2023, Direct synthesis of 8-fluorocaffeine and its transformation to 8-substituted caffeine, *ChemistrySelect*, 8, e202303074.

[28] Romero, A.H., Fuentes, G., Suescun, L., Piro, O., Echeverría, G., Gotopo, L., Pezaroglo, H., Álvarez, G., Cabrera, G., Cerecetto, H., and Couto, M., 2023, Tautomerism and rotamerism of favipiravir and

halogenated analogues in solution and in the solid state, *J. Org. Chem*., 88 (15), 10735–10752.

[29] Durán-Iturbide, N.A., Díaz-Eufracio, B.I., and Medina-Franco, J.L., 2020, *In silico* ADME/Tox profiling of natural products: A focus on BIOFACQUIM, *ACS Omega*, 5 (26), 16076–16084.

[30] Wu, F., Zhou, Y., Li, L., Shen, X., Chen, G., Wang, X., Liang, X., Tan, M., and Huang, Z., 2020, Computational approaches in preclinical studies on drug discovery and development, *Front. Chem*., 8, 726.

[31] Domínguez-Villa, F.X., Durán-Iturbide, N.A., and Ávila-Zárraga, J.G., 2021, Synthesis, molecular docking, and in silico ADME/Tox profiling studies of new 1-aryl-5-(3-azidopropyl)indol-4-ones: Potential inhibitors of SARS CoV-2 main protease, *Bioorg. Chem*., 106, 104497.

[32] Shityakov, S., and Förster, C., 2014, *In silico* predictive model to determine vector-mediated transport properties for the blood–brain barrier choline transporter, *Adv. Appl. Bioinf. Chem.*, 7, 23–36.

[33] Sugathan, K.J., Sreekumar, S., and Kamalan, B.C., 2024, *In silico* screening and identification of lead molecules from *Garcinia gummi-gutta* with multitarget activity against SARS-CoV-2, *J. Appl. Pharm. Sci.*, 14 (7), 124–132.

[34] Mishra, A., and Rathore, A.S., 2022, RNA dependent RNA polymerase (RdRp) as a drug target for SARS-CoV2, *J. Biomol. Struct. Dyn.*, 40 (13), 6039–60351.

[35] Wu, Y., Chang, K.Y., Lou, L., Edwards, L.G., Doma, B.K., and Xie, Z.R., 2020, *In silico* identification of drug candidates against COVID-19, *Inf. Med. Unlocked*, 21, 100461.

[36] Brunt, D., Lakernick, P.M., and Wu, C., 2022, Discovering new potential inhibitors to SARS-CoV-2 RNA dependent RNA polymerase (RdRp) using high throughput virtual screening and molecular dynamics simulations, *Sci. Rep*., 12 (1), 19986.

[37] Hollingsworth, S.A., and Dror, R.O., 2018, Molecular dynamics simulation for all, *Neuron*, 99 (6), 1129–1143.